Efficient Schottky-quantum-dot photovoltaics: The roles of depletion, drift, and diffusion

Keith W. Johnston, Andras G. Pattantyus-Abraham, Jason P. Clifford, Stefan H. Myrskog, Sjoerd Hoogland, Harnik Shukla, Ethan J. D. Klem, Larissa Levina, and Edward H. Sargent[a)]

Department of Electrical and Computer Engineering, University of Toronto, 10 King's College Rd., Toronto, Ontario M5S 3G4, Canada

(Received 26 January 2008; accepted 20 February 2008; published online 27 March 2008)

PbS colloidal quantum dot photovoltaic devices in a Schottky architecture have demonstrated an infrared power conversion efficiency of 4.2%. Here, we elucidate the internal mechanisms leading to this efficiency. At relevant intensities, the drift length is 10 μm for holes and 1 μm for electrons. Transport within the 150 nm wide depletion region is therefore highly efficient. The electron diffusion length of 0.1 μm is comparable to neutral region width. We quantitatively account for the observed 37% external quantum efficiency, showing that it results from the large depletion width and long carrier lifetime combined. © *2008 American Institute of Physics*.
[DOI: 10.1063/1.2896295]

Solution-processed photovoltaics offer the possibility of low-cost, large area solar cells. This field is underpinned by advances in small-molecule organic and polymeric semiconductors, which have recently led to solar (AM1.5) power conversion efficiencies in excess of 6%.[1] Organic and polymer photovoltaic devices typically absorb strongly in the visible regime but leave a large portion of the infrared untapped: the smallest-bandgap conjugated polymers have exhibited sensitivity only to 1000 nm.[2] It is imperative to utilize solution-processable materials with smaller bandgaps to harness solar energy efficiently.[3]

PbS and PbSe quantum dots offer sensitivity well into the short-wavelength infrared.[4,5] In photovoltaic devices incorporating these materials,[6–8] it was assumed that a donor-acceptor interface was crucial for the charge separation process. In contrast, we have developed photovoltaic devices based on a Schottky barrier between a *p*-type PbS nanocrystal film and a low work function metal that achieved power conversion efficiencies of up to 4.2% under infrared illumination.[9] Further, the internal quantum efficiency was observed to exceed 90%, suggesting efficient carrier transport and extraction.

Here, we investigate Schottky-quantum-dot photovoltaic devices with the goal to understand how charge carriers are transported and extracted. This letter builds on previous studies of planar metal/nanocrystal/metal structures.[7,8,10] The charge transport characteristics are investigated by extracting various material parameters including carrier mobilities. These parameters, coupled with recombination-limited lifetime data, are then used to explain the high charge extraction efficiency in these devices.

Photovoltaic devices were prepared as reported elsewhere.[9,11] Briefly, the PbS nanocrystals with a first absorption peak at ~1650 nm, corresponding to a diameter of ~6 nm, were prepared using an organometallic route.[12] The ~2.5 nm long oleate ligands coating the nanocrystal surfaces were partially exchanged to ~0.6 nm long *n*-butylamine ligands over three days. Nanocrystal films were spin coated on indium tin oxide (ITO)-coated glass substrates from a 150 mg mL^{-1} octane solution before being capped with 140 nm Al/190 nm Ag deposited by thermal evaporation. A Schottky barrier is formed at the junction between thermally deposited Al and the *p*-type PbS colloidal nanocrystal film.[11] This provides a mechanism for photogenerated charge separation and transport.

We propose to model the macroscopic behavior of quantum dot film as a homogeneous medium having an effective doping, electron and hole mobility, and band alignments. In this framework, we represent the aggregate behavior of the film using a conventional band diagram (Fig. 1).

Carrier extraction by linearly increasing voltage (CELIV) was used to extract hole mobility and static relative permittivity.[13] We applied a linearly increasing voltage to various photovoltaic devices (300–600 nm thick) in reverse bias (i.e., Al at a higher potential than ITO) and monitored the current signal through a 50 Ω load. *RC* time constants were observed to be at least a factor of 10 smaller than the time scales of interest.

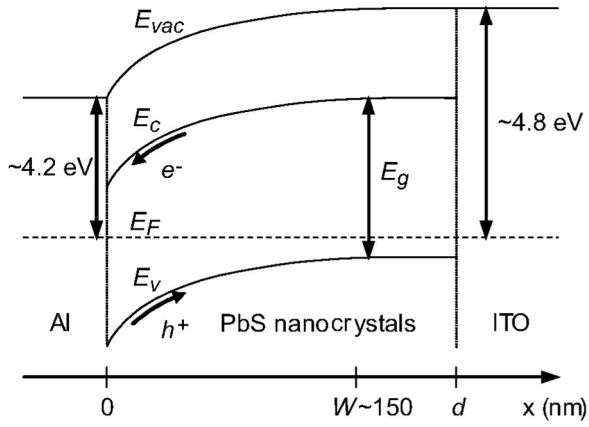

FIG. 1. The energy band model, showing the presence of a Schottky barrier and bending in the conduction band (E_c), valence band (E_v), and vacuum energy level (E_{vac}) near the Al/nanocrystal interface. The built-in electric field within the depletion region of the nanocrystal layer governs the transport of photogenerated electrons (e^-) and holes (h^+). The Fermi level (E_F) is drawn to show the *p*-type conduction characteristics. The bandgap (E_g) of these nanocrystals is ~0.75 eV, defined as the first absorption peak energy.

a)Author to whom correspondence should be addressed. Electronic mail: ted.sargent@utoronto.ca.

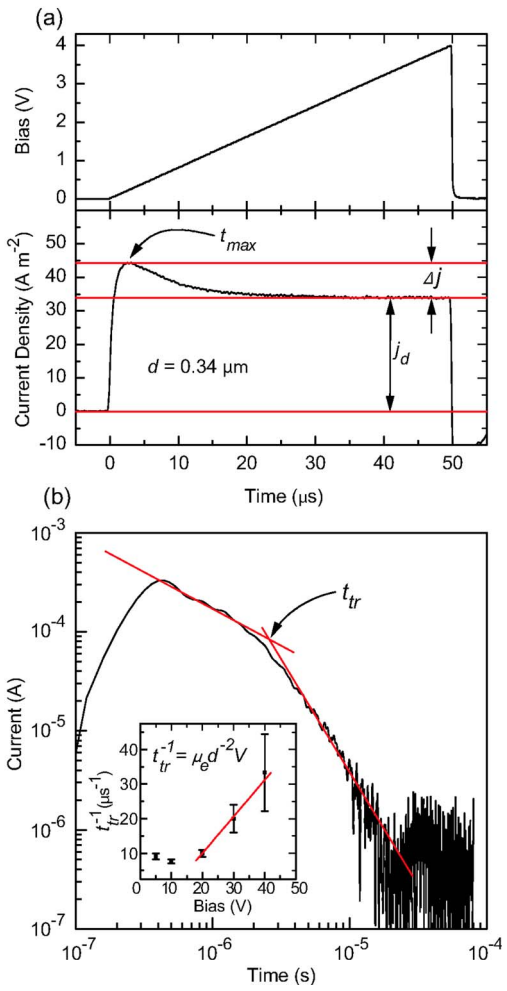

FIG. 2. (Color online) Representative current transient signals used to extract (a) the hole mobility (CELIV, under 80 000 V s^{-1} ramp rate) and (b) the electron mobility (time-of-flight, under 40 V bias). The inset shows the bias dependence of the transit time (t_{tr}). The slope of the data above 15 V was used to determine the mobility. The dashed red lines represent in (a) the different current density levels and in (b) the least-squares fits to the data.

Figure 2(a) shows a representative CELIV transient at a ramp rate (A) of 80 000 V s^{-1}. The majority carrier mobility can be extracted from the time required for the transient current signal (i.e., due to equilibrium charge extraction) to reach its maximum value t_{max} according to[13]

$$\mu_h = \frac{2d^2}{3At_{max}^2\left(1 + 0.36\frac{\Delta j}{j_d}\right)}, \tag{1}$$

where μ_h is the hole mobility, d is the device thickness, j_d is the displacement current, and Δj is the maximum drift current. In this manner, the hole mobility was found to be $(1.5 \pm 0.1) \times 10^{-3}$ cm^2 V^{-1} s^{-1}.

After the decay of the transient drift component, the current signal consisted entirely of the displacement component j_d. By relating this to device and material parameters,[13] we determined the static relative permittivity ε_r to be 17 ± 2 for the PbS nanocrystal films.

We characterized the depletion region of the Schottky junction using capacitance-voltage measurements directly on photovoltaic devices.[11] Using a Mott–Schottky analysis, we estimated the acceptor density to be 3×10^{16} cm^{-3} and the built-in potential V_{bi} was found to be 0.3 V.[11] The capacitance data at zero bias indicated a depletion width W of ~150 nm under short-circuit conditions (using $\varepsilon_r = 17$).

We then sought to obtain minority carrier (electron) mobilities using time-of-flight techniques in optically thick samples.[14] Time-of-flight transients were obtained by illuminating the devices through the ITO contact with a 10 ns pulse at 532 nm using an yttrium aluminum garnet laser. Devices were reverse biased to isolate the electron transport dynamics. The transient current across a 50 Ω load was observed on a digital oscilloscope. The nanocrystal film thickness was 1.6 ± 0.1 μm, which is much greater than the absorption depth (~200 nm) at the laser wavelength. The charge extracted was less than 10% of the capacitive charge. In addition, the RC time constant of the system was calculated to be much smaller than the time scales of interest.

A representative time-of-flight transient is shown in Fig. 2(b). The transport was observed to be dispersive in nature; therefore, the intersection time of the transient asymptotes was used to determine the transit time.[14] The bias dependence of the transit time is shown in the inset of Fig. 2(b). A change in slope appears above a bias of 15 V (a field of 9.4×10^4 V cm^{-1}). We interpret this as the bias at which the device becomes fully depleted and, thus, the electric field becomes uniform throughout the film. In the fully depleted regime, the electron mobility (μ_e) was found to be $(2 \pm 1) \times 10^{-4}$ cm^2 V^{-1} s^{-1}, which is comparable to that reported for CdSe and PbSe nanocrystals.[15,16]

The recombination-limited lifetime was measured using the decay of the open-circuit voltage (V_{oc}) following illumination turn off.[17,18] For these measurements, ~200 nm thick devices were illuminated with a 975 nm diode laser at room temperature, which was modulated using a digital pulse generator. The laser turn-off time was measured to be 3 μs. The transient responses were measured using an oscilloscope with 1 MΩ input impedance. Figure 3(a) shows a typical V_{oc} decay curve at 16 mW cm^{-2} illumination.

The initial slope of the decay curve dV_{oc}/dt is related to the recombination-limited lifetime (τ) by[18]

$$\tau = -\frac{kT}{q}\frac{F_I}{\frac{dV_{oc}}{dt}}, \tag{2}$$

where k is the Boltzmann constant, T is temperature, q is the elementary charge, and F_I ranges between 1 at low injection and 2 at high injection. In these calculations, we used an acceptor density of 3×10^{16} cm^{-3} and assumed that all absorbed light (~30% of the incident light for a 200 nm device) was converted into free carriers.

The lifetime was determined over a wide range of intensities and it is shown along with the external quantum efficiency (EQE) data for the same device in Fig. 3(b). The lifetime decreased steadily from 1 ms at low intensities to 10 μs at high intensities. The device EQE was constant at low intensities and dropped pronouncedly at intensities above 10 mW cm^{-2}. The dramatic decline of EQE at high intensities begins when the lifetime drops below the photocarrier extraction time.

At a wavelength of 975 nm, light absorption and concomitant exciton generation occur uniformly throughout the device. Holes and electrons diffuse due to concentration gradients and drift under the internal electric field. The carrier

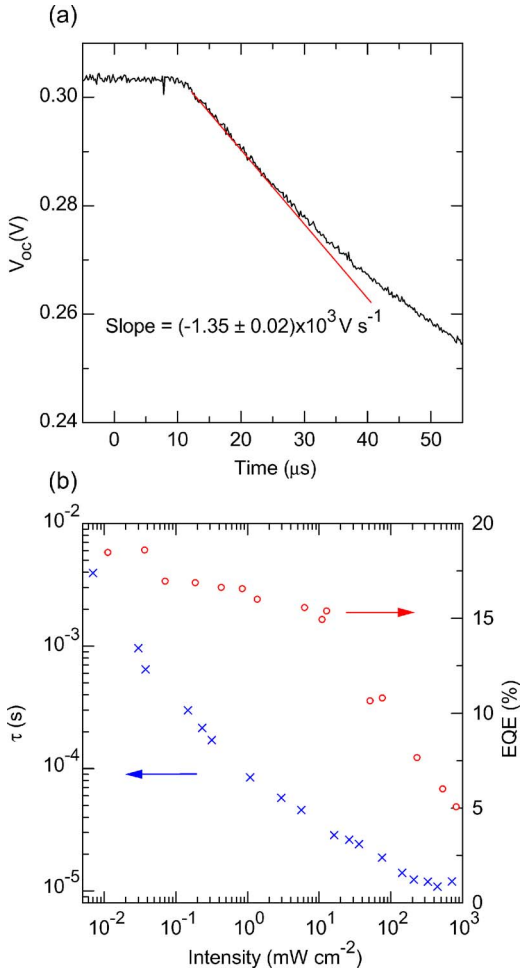

FIG. 3. (Color online) (a) Representative V_{oc} decay signal (after 975 nm, 16 mW cm^{-2} illumination turn off) and a linear best fit (dashed red line) used to determine the recombination-limited lifetime. (b) Lifetime (blue crosses, left axis) and EQE (red circles, right axis) and as a function of illumination intensity at 975 nm. A knee can be seen in the EQE plot at ~10 mW cm^{-1}, which corresponds to the intensity at which the minority carrier transit time exceeds the lifetime. The scatter in the data at low intensities is due to larger measurement uncertainty.

diffusion length under short-circuit conditions is given by $l_{\text{diff}}=\sqrt{\mu\tau kT/q}$.

The drift length is calculated by approximating the linearly varying electric field in the depletion region by its average value[19] $l_{\text{drift}}=\mu\tau V_{\text{bi}}/W$.

At 12 mW cm^{-2}, the lifetime is ~36 μs. The built-in potential of these devices leads to hole and electron drift lengths of 10 and 1 μm, respectively, which are well in excess of the depletion width. The diffusion lengths were estimated to be 0.4 and 0.1 μm for holes and electrons, respectively.

The above considerations allow us to present a picture of device internal operation. Most of the carriers are generated, and efficiently separated, in the wide depletion region (~150 nm). The built-in field drives electrons to the Al interface, while holes drift to the edge of the depletion region and diffuse to the ITO interface. Efficient device operation depends on the balance between light absorption and efficient carrier extraction; a thick active layer may absorb more light and generate additional carriers but those generated near either contacts can have a transit time to the opposing contact that exceeds the lifetime. In efficient devices, the depletion region accounts for the majority of the device thickness (230 nm for the best reported device). These devices showed an EQE of 37% at 975 nm, while absorbing 41% of the incident light. Assuming a uniform absorption profile, 27% of the incident light is absorbed in the depletion region and these photogenerated carriers are extracted efficiently. The remaining 14% of the light is absorbed in the neutral region and a fraction (~25%) of this component is lost to carrier recombination.

In thicker devices, the efficiency is limited by the rate of carrier diffusion through the neutral region. This becomes significant when the device thickness is approximately equal to the sum of the minority carrier (electron) diffusion length and the depletion width. Indeed, a decline in efficiency was observed for thicknesses above 300 nm.

Two separate phenomena—the long recombination-limited lifetime and wide depletion region—are thus critically important for efficient charge separation and extraction in these devices. Each is traceable ultimately to the bulk properties of PbS. The depletion width is determined by the interplay between acceptor density and static relative permittivity. The large value of the latter (17 in these materials) is due to the correspondingly large static relative permittivity of bulk PbS (~160),[20] which is specific to lead chalcogenides among semiconductors used for photovoltaic applications. Bulk PbS has been shown to exhibit long carrier lifetimes[21] consistent with those reported herein.

The authors wish to thank S. Hinds, G. Koleilat, and G. Konstantatos for helpful discussions. This research was supported by the Natural Sciences and Engineering Research Council of Canada.

[1] J. Y. Kim, K. Lee, N. E. Coates, D. Moses, T. Nguyen, M. Dante, and A. J. Heeger, Science **317**, 222 (2007).
[2] M. M. Wienk, M. G. R. Turbiez, M. P. Struijk, M. Fonrodona, and R. A. J. Janssen, Appl. Phys. Lett. **88**, 153511 (2006).
[3] A. Martí and G. L. Araújo, Sol. Energy Mater. Sol. Cells **43**, 203 (1996).
[4] G. Konstantatos, J. Clifford, L. Levina, and E. H. Sargent, Nat. Photonics **1**, 531 (2007).
[5] F. Wise, Acc. Chem. Res. **33**, 773 (2000).
[6] S. A. McDonald, G. Konstantatos, S. Zhang, P. W. Cyr, E. J. D. Klem, L. Levina, and E. H. Sargent, Nat. Mater. **4**, 138 (2005).
[7] A. Maria, P. W. Cyr, E. J. D. Klem, L. Levina, and E. H. Sargent, Appl. Phys. Lett. **87**, 213112 (2005).
[8] E. J. D. Klem, D. D. MacNeil, P. W. Cyr, L. Levina, and E. H. Sargent, Appl. Phys. Lett. **90**, 183113 (2007).
[9] K. W. Johnston, A. G. Pattantyus-Abraham, J. P. Clifford, S. H. Myrskog, D. D. MacNeil, L. Levina, and E. H. Sargent, "Schottky-quantum dot photovoltaics for efficient infrared power conversion" (unpublished).
[10] D. S. Ginger and N. C. Greenham, J. Appl. Phys. **87**, 1361 (2000).
[11] J. P. Clifford, K. W. Johnston, L. Levina, and E. H. Sargent, Appl. Phys. Lett. **91**, 253117 (2007).
[12] M. A. Hines and G. D. Scholes, Adv. Mater. (Weinheim, Ger.) **15**, 1844 (2003).
[13] G. Juska, M. Viliunas, K. Arlauskas, N. Nekrasas, N. Wyrsch, and L. Feitknecht, J. Appl. Phys. **89**, 4971 (2001).
[14] P. Borsenberger and D. Weiss, *Organic Photoreceptors for Xerography* (Dekker, New York, 1998).
[15] D. Yu, C. Wang, and P. Guyot-Sionnest, Science **300**, 1277 (2003).
[16] D. V. Talapin and C. B. Murray, Science **310**, 86 (2005).
[17] A. Zaban, M. Greenshtein, and J. Bisquert, ChemPhysChem **4**, 859 (2003).
[18] J. E. Mahan, T. W. Ekstedt, R. I. Frank, and R. Kaplow, IEEE Trans. Electron Devices **26**, 733 (1979).
[19] E. H. Rhoderick and R. H. Williams, *Metal-Semiconductor Contacts* (Clarendon, Oxford, 1988).
[20] M. M. Sokoloski and P. H. Fang, Phys. Lett. **16**, 222 (1965).
[21] W. Scanlon, Phys. Rev. **106**, 718 (1957).